JOURNAL OF GEOPHYSICAL RESEARCH, VOL. 112, A05222, doi:10.1029/2006JA012126, 2007

EL - a possible indicator to monitor the magnetic field stretching at global scale during substorm expansive phase: Statistical study

M. Meurant,[1] J.-C. Gérard,[2] C. Blockx,[2] E. Spanswick,[1] E. F. Donovan,[1] B. Hubert,[2] V. Coumans,[2] and M. Connors[3]

Received 17 October 2006; revised 29 January 2007; accepted 8 February 2007; published 26 May 2007.

[1] An interesting open question of magnetospheric physics is the understanding of the dynamics of the magnetotail. The question of the field stretching is even more challenging during substorm periods, mainly because of the short time scales involved during such explosive events. In this study, we asses the ability of global scale proton auroral imaging to provide information on the tail stretching during active periods. We base our investigation on more than 250 isolated substorms observed by IMAGE-SI12 between 2000 and 2002. Applying the algorithm proposed by Donovan et al. (2003) for ground based observations to IMAGE-SI12 data, we determine the Equatorial Limit (EL) of the oval and propose to use it as an indicator of the tail stretching. Simultaneous comparison with GOES-8 allows us to estimate how strong is the relationship between the EL position deduced from SI12 and the magnetic field stretching. The EL indicator is shown to be consistent with previous studies (Sergeev and Gvozdevsky (1995) and Blockx et al. (2005)) and is found to be located in average $\sim$1 degree equatorward of the limit deduced from DMSP measurements. The time evolution of the EL magnetic latitude is also presented for different local times relative to the onset position. This evolution of the EL index presents an asymmetric shape following the time of onset, suggesting a more important stretching of the tail duskward of the onset position. This asymmetric stretching is consistent with GOES-8 in situ measurements.

Citation: Meurant, M., J.-C. Gérard, C. Blockx, E. Spanswick, E. F. Donovan, B. Hubert, V. Coumans, and M. Connors (2007), EL - a possible indicator to monitor the magnetic field stretching at global scale during substorm expansive phase: Statistical study, *J. Geophys. Res.*, *112*, A05222, doi:10.1029/2006JA012126.

1. Introduction

[2] The determination of the morphology of the Earth's magnetosphere under particular conditions is one of the main challenges of magnetospheric sciences. One of the most significant tools to provide such topology is the set of empirical models based on magnetic field statistical observations proposed by *Tsyganenko* [eg. 1989, 1996]. However, it is generally accepted that results obtained with such global models are not reliable during active periods such as substorm expansive phase. Another estimator of the field stretching is based on the isotropic boundary (IB) deduced from the observation of precipitating particles. The isotropic boundary is the field-aligned surface which separates the region of the magnetosphere where protons bounce between mirror points without (or with a low) scattering (adiabatic motion) and the region where the pitch angle scattering is efficient enough to keep the loss cone full (non-adiabatic behavior) [*Sergeev and Gvozdevsky*, 1995]. The IB is known to correlate well with the magnetic field inclination at geosynchronous orbit around 00 MLT and therefore provides a way to monitor magnetotail stretching. Several ways to identify the IB position using different proxies have been proposed in the literature. Based on *in situ* spacecraft data, *Sergeev and Gvozdevsky* [1995] have defined the IB position using NOAA data while *Newell et al.* [1996] defined a comparable boundary (the b2i boundary) based on Defense Meteorological Satellite Program (DMSP) data. *Donovan et al.* [2003] used ground-based meridian scanning photometers (MSP) to determine the "optical b2i". In complement to these methods, an IB determination on a wide range of magnetic local time (MLT) with a high temporal resolution is useful. Recently, *Blockx et al.* [2005] have demonstrated the potential to use SI12 data to monitor the magnetotail stretching during quiet periods. However, it has not been demonstrated that ionospheric measurements allow monitoring of the magnetospheric topology during active periods. During quiet periods, proton precipitation on the nightside is well related to the amount of tail stretching. It is consequently not surprising that the magnetic field topology may be deduced from precipitated proton fluxes. During active periods however, significant precipitation can occur when a) particles with isotropic pitch angle distributions are injected in the region of closed field

[1] Institute for Space Research, University of Calgary, Calgary, Canada.
[2] Laboratoire de physique atmosphérique et planétaire, Université de Liège, Liège, Belgium.
[3] Athabasca University, Edmonton, Canada.

0148-0227/07/2006JA012126$09.00

lines (dayside reconnection or nightside substorm injection process), b) electric fields (dc or waves) interact with stably trapped particles to scatter them into the loss cone, c) magnetic reconfiguration compress the volume of the field/flux region (compression) or d) when particles are scattered in stretched field line configuration e.g. during substorm growth phase [*Mende et al.*, 2002]. The first three mechanisms are superimposed to the field line topology effect and in these cases, characteristics of the observed proton auroral are not only determined by field stretching.

[3] The objective of this paper is to assess, on a statistical basis, whether it is possible to retrieve information about the geotail stretching during active periods from global scale auroral optical data, or, in other words, if tail stretching exerts a major control on auroral emission characteristics during substorm expansive phase.

[4] During quiet periods, IB or its proxies are used to obtain information on the tail stretching. By analogy, we use here the technique proposed by *Donovan et al.* [2003] to deduce the optical b2i position. We apply this algorithm to data provided by the SI12 proton imager [*Mende et al.*, 2000] on board the IMAGE spacecraft, taking advantage of the two minute resolution and the global coverage of these data. This approach allows the determination of the boundary position simultaneously at different magnetic local times (MLT). However, even if Donovan's algorithm was designed to identify a proxy of IB, because of the high level of activity during substorm periods, it is not demonstrated that the boundary defined with this algorithm during substorm periods still separates regions where protons presents an adiabatic motion and those where they present a non-adiabatic motion. In order to avoid confusion with the physical meaning of IB, we will rather use the terminology ''oval's Equatorial Limit (EL)'' to identify the limit provided by the Donovan's algorithm and consider it as a potential indicator of field stretching and not as a boundary between two physically different regions of the tail. The indicator used to estimate the tail stretching is the elevation angle deduced from GOES-8 measurements. The elevation angle is the angle between the Earth-spacecraft line and the magnetic field. Consequently, the smaller the elevation angle, the more stretched the magnetic field.

[5] After a brief description of the data and the applied method (section 2), we investigate the relation between the position of EL and the magnetic field stretching (section 3.1). These results are also compared to previous studies. In the section 3.2 we present the comparison of the EL and the b2i boundary positions in order to assess what is the discrepancy between positions deduced by Donovan's algorithm applied on global data and *in situ* measurements recorded by DMSP. In section 4, we finally apply the method to a case study and a large set of substorms to describe the behavior of EL at different MLT's during the substorm expansive phase.

2. Data

2.1. Image Data

[6] The FUV instrument [*Mende et al.*, 2000] onboard the IMAGE satellite provides three simultaneous snapshots with approximately the same field of view of the auroral region and a 2 min time resolution. The SI12 instrument has a grill system to reject the geocoronal Ly-α emission at 1215.6 Å and allow a fraction of the broad auroral Ly-α line profile. The FUV-SI12 camera is sensitive to the Doppler-shifted Lyman-α auroral emission and provides images with a spatial resolution of $\sim$100 km from apogee. Taking advantage of the Doppler shift, the geocoronal emission is suppressed and only proton induced emission is measured. When protons penetrate the atmosphere, they are slowed down by elastic and inelastic collision with neutral constituents. During some of these collisions, the proton capture an electron, leaving a fast hydrogen atom, possibly in an excited state. If the excited hydrogen atoms move toward the ground-based observer, the photon is emitted with a Doppler shift from the line center at rest. The observed line profile is the result of the integration of the contributions of all velocity vector projections on the line of sight. The other two snapshots provide images of the electron induced N_2 LBH emissions in the 140 – 180 nm band (WIC) and in a 5-nm region centered on the OI line at 135.6 nm (SI13). Pixels size are 70x70 km^2 for WIC and 140x140 km^2 for SI13 from apogee.

[7] Substorm events used for this study are selected in the list given by *Frey et al.* [2004]. This list provides times and positions of all onsets observed with the WIC camera. From this list, we selected only isolated events which are entirely observed by IMAGE-FUV. We defined an ''isolated event'' as an event separated from the previous and the next one by at least two hours. Such isolated events are added to our list only if it is entirely observed, i.e. if FUV data are available from 90 min before to 90 min after onset with a delay of at most 10 minutes between two consecutive images (i.e. 5 consecutive missing images). Data containing dark bands (due to a mass memory problem in the spacecraft) and too small field of view of the nightside (due to a non-favorable geometry of observation) are also excluded. The requested coverage is the 2100-0300 MLT – 60°-90° MLAT sector which must be filled during the 90 min before to 90 min after the onset. In addition to those conditions, some visual criteria are also applied to define the set of substorms used for this study. To be considered, an event has to satisfy these following criteria: suitable data (a) have a signal/noise ratio that allows the oval to be distinguished from the background, (b) correct pointing data: an event is rejected if the coordinate grid presents obvious anomalous displacement between two consecutive images or if the oval is badly positioned on the coordinate grid, (c) avoid data with view angle distorting single pixels and making them as large as the oval (due to bad viewing angles); and (d) the top of SI12 images may present a very bright band. An event is therefore rejected if those bands are in the field 21-03 MLT – 60-90 MLAT. These restrictions decrease the number of events compared to the *Frey et al.* [2004] list from 2437 to 259 events. Onset positions of the selected substorms are described by histograms displayed on Figure 1. Figure 1a shows the distribution of onset positions observed by the WIC camera. The mean value of this distribution is 23.13 MLT. Figure 1b displays the latitudinal distribution of onsets, and present a mean value of 66.31° MLAT.

[8] Values obtained for this sample are close to typical values generally reported for substorms onsets as presented by *Gérard et al.* [2004], (their Table 1).

[9] Several steps are needed to deduce the position of the EL of the oval from SI12 data. The first step is a subtraction

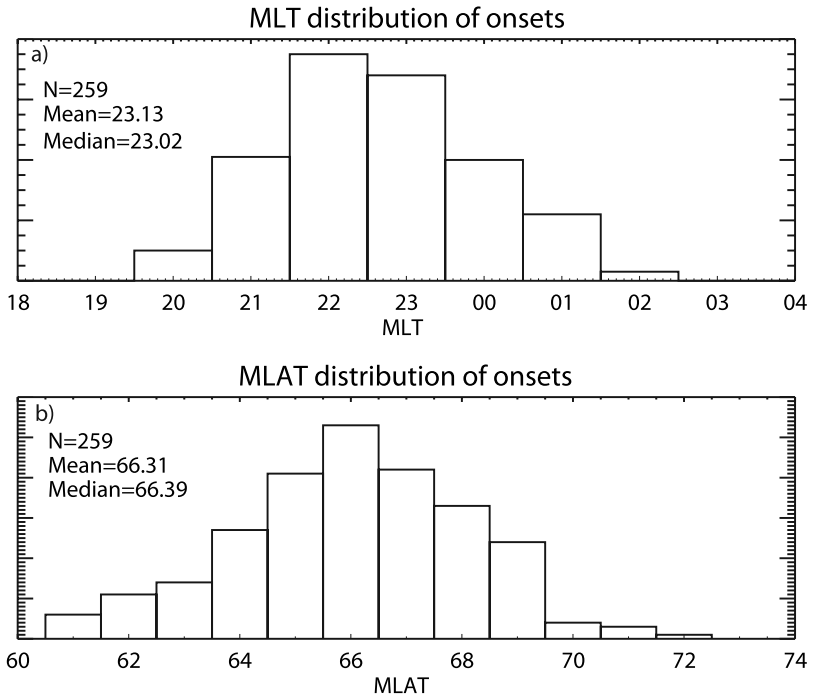

Figure 1. (a) Histogram of the MLT positions of the selected substorm onsets. (b) Histogram of the MLAT distribution of the onsets of the selected events.

of the small background observed in the SI12 data. The subtraction method was previously used in *Hubert et al.* [2006] and references therein. In a second step, the 50°-90° MLAT – 2000-0400 MLT sector of the SI12 "clean images" are transformed in a MLAT – MLT keogram with a resolution of 0.5 hour MLT and 1° MLAT. MLT profiles extracted from these keograms are then approximated by a Gaussian fit of the form

$$f(MLAT) = A_0 e^{\frac{-z^2}{2}} + A_3$$

with

$$z = \frac{MLAT - A_1}{A_2}$$

where A_i (i = 0,1,2 or 3) are constants determined by the least square fit method. The last step is the determination of the magnetic latitude of the EL. We assume that this boundary is located 1.4σ equatorward of the Gaussian fit maximum as suggested by *Donovan et al.* [2003] for similar fits. In this way, each SI12 image provides 17 determinations of the EL positions in the interval 2000 – 0400 MLT every two minutes. Figure 2 provides an illustration of the EL position

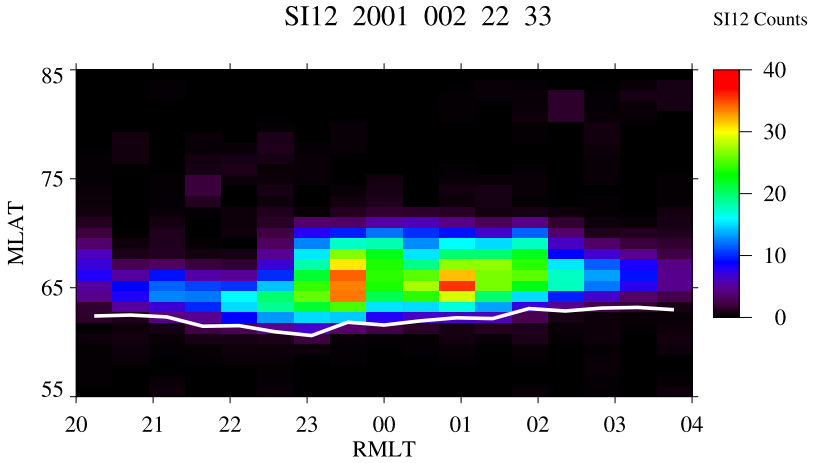

Figure 2. SI12 data displayed in keogram (2001 Jan 02 at 2233 UT). The solid line represents the EL position determined by the Donovan's algorithm. The color scale represents the intensity measured by the SI12 instrument for each MLT – MLAT location.

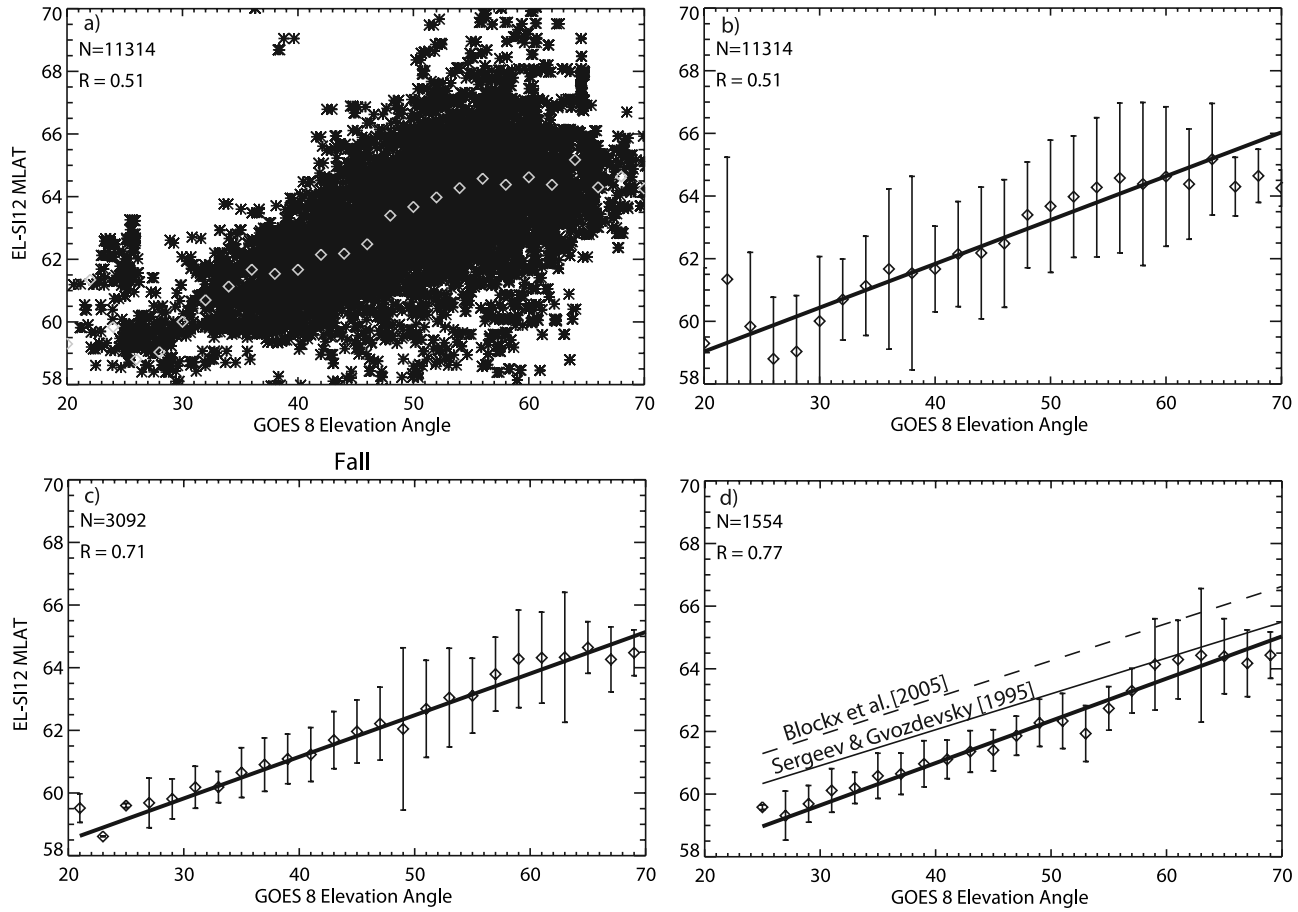

Figure 3. (a) Scatter plot of the 11314 elevation angles deduced from GOES 8 measurements in the 21 – 03 MLT sector vs the magnetic latitude of EL deduced from SI12 data at the same MLT. These measurements were made by GOES-8 between 90 minutes before to 90 minutes after the onset. Squares represent the mean value of the $EL_{\ddot{E}}$ of the oval for two degrees bins of the elevation angle. (b) The average values obtained with two degree bins are reproduced for the comparison with error bars representing a 1σ deviation. The solid line represents the linear regression of the entire sample presented in (a). (c) Same plot than 3b, but restricted to the fall periods. (d) Same plot as 3b but restricted to substorms observed in December 2000 and 2001. The thin line is the regression obtained by *Sergeev and Gvozdevsky* [1995] and the dashed line is obtained by the method developed by *Blockx et al.* [2005] and applied to the substorms of December 2000 and 2001.

determined from SI12 data during the substorm which occurred on January 02, 2001. Each profile is fitted by a Gaussian and the position located at 1.4σ equatorward of the maximum is represented by the position of the white curve.

2.2. Goes Data

[10] The GOES-8 satellite is a geosynchronous spacecraft carrying a magnetometer providing continuous measurements of the Earth's magnetic field. To monitor the magnetic field stretching during substorm events, we use the magnetic field elevation angle, defined as $E_l = \text{atan}(B_p/B_e)$ with B_e, the magnetic field parallel to the satellite-Earth center line and points earthward and B_p the magnetic field parallel to the satellite spin axis (perpendicular to the satellite's orbital plane). The inclination angle I_{dip} measured at magnetic latitude λ in a dipolar field is given by

$$\tan I_{dip} = 2 \tan \lambda.$$

[11] If the geomagnetic field were dipolar the elevation angle would be 69.1°. This E_{ldip} value is therefore the limit below which the magnetic field lines are stretched (in the nightside) and beyond which they are compressed (on the dayside). To infer the relation between the magnetic field elevation angle and the position of EL (see section 3.1), we use all available GOES-8 data during substorm events selected as described above, when GOES-8 was in the 2100 – 0300 MLT sector. The relation between the elevation angle deduced from GOES-8 data and the EL position is affected by a seasonal effect on the elevation angle mean value. This aspect is discussed in section 3.1 which compares the EL position and the GOES-8 elevation angle.

2.3. DMSP Data

[12] Spectrograms recorded by the SSJ/4 detectors on board the DMSP spacecraft make it possible to identify several boundaries like the b2i boundary, which is a good proxy of the IB [*Newell et al.*, 1998]. In order to evaluate

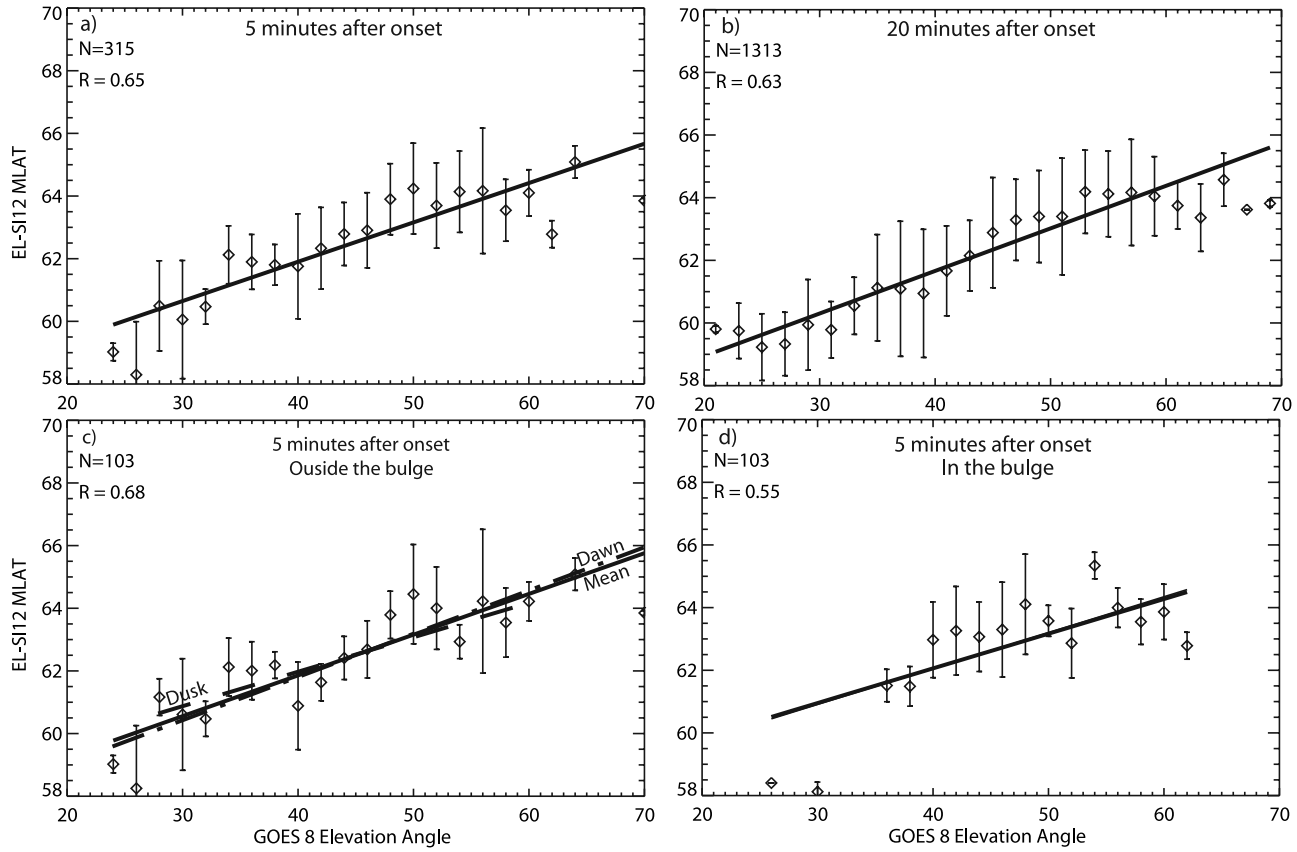

Figure 4. Same as Figure 3b but for data collected during the 5 minutes (a) and 20 minutes (b) after onset. (c) Same as Figure 4a for MLT positions located outside the bulge. The dashed line is for MLT located duskward of the bulge and the dashed-dotted line is for MLT located dawnward of the bulge. (d) Same as Figure 4a for MLT positions located in the bulge.

the difference between the EL position determined with SI12 data and b2i positions determined by DMSP crossing (see section 3.2), we have selected 299 DMSP crossings in the 2000 – 0400 MLT sector in the −90 min to +90 min period around onset. Each of these crossings provides the MLAT and MLT of each b2i determination. Because of the DMSP orbital configuration, all of these 299 crossings are confined to the 2000 – 21.60 MLT sector.

3. Validation of the Method During Active Periods

[13] SI12 data were previously used by *Blockx et al.* [2005] to monitor the magnetotail stretching. However, this study did not consider active periods, such as substorm expansive phases. Before SI12 data can be used to determine the equatorward boundary of the oval, one needs to assess the ability of these data to reach this goal. We proceed in two steps. The first step consists in verifies that EL position provided by SI12 is correlated with the magnetic field stretching. In this study, we use the elevation angle measured by the GOES-8 satellite as a proxy of the magnetic tail stretching. The second step is to evaluate how close the EL values deduced from SI12 are to the DMSP-b2i boundary, which is a commonly accepted proxy for IB [*Newell et al.*, 1998].

3.1. Comparison With GOES Data

[14] The elevation angles deduced from measurements recorded by GOES-8 in the 2100 – 0300 MLT sector during selected substorm events are displayed in Figure 3. For each point of this plot, the EL position is taken at the GOES-8 longitude. Figures 3a and 3b present the relation between GOES-8 elevation angle and the latitude of EL obtained during 90 minutes before to 90 minutes after onset for the set of 259 substorms. A dependence is observed between these two quantities (the linear regression gives a value of r = 0.51). The observed scatter is typically ∼4 degrees which can be partially attributed to the seasonal variation of the distance between GOES and the neutral sheet. To illustrate the seasonal effect, Figure 3c represents the same plot as 3a and b but restricted to the fall season, which contributes to decrease the scatter. In Figure 3d we compare the linear regression obtained for substorms observed during December 2000 and 2001 with that given by *Sergeev and Gvozdevsky* [1995] and those obtained from the *Blockx et al.* [2005] method applied to the set of substorms observed during the same period. The linear regression in Figure 2d presents a slope similar to that obtained by *Sergeev and Gvozdevsky* [1995]. In the *Sergeev and Gvozdevsky*'s study, this regression represents the dependence of the IB magnetic latitude to the elevation angle. The EL determined by the Donovan's algorithm does not have the same physical

meaning when used during active periods, because of the mechanisms modifying the precipitated fluxes characteristics along field lines, as mentioned in section 1, It is nevertheless used as indicator of the tail stretching. However, in this statistical comparison, the dependence of these two limits to the magnetospheric stretching appears close. Results obtained with the *Blockx et al.* method present a slope comparable to those obtained in the *Sergeev and Gvozdevsky*'s and the present study, but with a shift of $\sim$1.5 degrees. The limit used by the *Blockx et al.* method is defined as the maximum of intensity of the MLAT profile, located poleward of EL, which explains the existence of the shift observed in Figure 3d.

[15] As observed in Figure 4a and b, the trend is essentially the same if the sample is restricted to different time periods. Figure 4a represents the values limited to the 5 minutes after the onset and Figure 4b to the 20 minutes after onset. Figures 4c and 4d distinguish between measurements made outside and in the bulge (the bulge is the auroral local intensification of a pre-existing quite arc around the onset position). The regressions obtained from these two subsets are similar than those observed in Figure 4a. Dashed and dashed-dotted lines represent equivalent regressions for regions located respectively duskward and dawnward of the bulge, which present similar slopes.

3.2. Comparison With DMSP Data

[16] In order to determine, on a statistical basis, how far the EL deduced from SI12 is from b2i, we now compare EL and b2i positions for 299 DMSP crossings through the auroral oval. As mentioned in Section 2.3, due to DMSP orbits configuration, DMSP measurements are recorded in the 2000 – 21.60 MLT sector. This sector is typically located duskward of the bulge. Each point of Figure 5a represents one DMSP crossing: the vertical axis indicates the position of b2i and the horizontal axis shows the MLAT of EL at the DMSP local time. As seen in this plot, the MLAT of b2i is generally located at higher latitudes than EL. This shift is summarized in plot 5b. The histogram presented in Figure 5b indicates the distance (in degree) between b2i determined by DMSP and EL determined by SI12. The distribution is not symmetric around zero with more than 80% of MLAT values provided by DMSP higher than those deduced from SI12. About 72% of the boundary determinations are within a $\pm 1.5^\circ$ interval. A 1.5° distance roughly implies 165 km at the 110 km altitude level. Knowing that the SI12 resolution is $\sim$130 km when the spacecraft is at apogee and considering PSF effects and pointing uncertainties, this difference between b2i and EL positions appears reasonably small. On individual events however, this difference may be larger.

[17] The comparison between the EL position and elevation angles deduced from GOES-8 shows a clear dependence between these two quantities. Moreover, this dependence appears to be in good agreement with *Sergeev and Gvozdevsky* [1995] and *Blockx et al.* [2005] results. Comparison with GOES-8 data indicates that EL may be considered as a useful tool to evaluate the stretching of the nightside field.

[18] Comparisons with b2i positions deduced from DMSP crossings show that the EL_Λ is typically located about 1 degree equatorward of b2i. The fact that these two

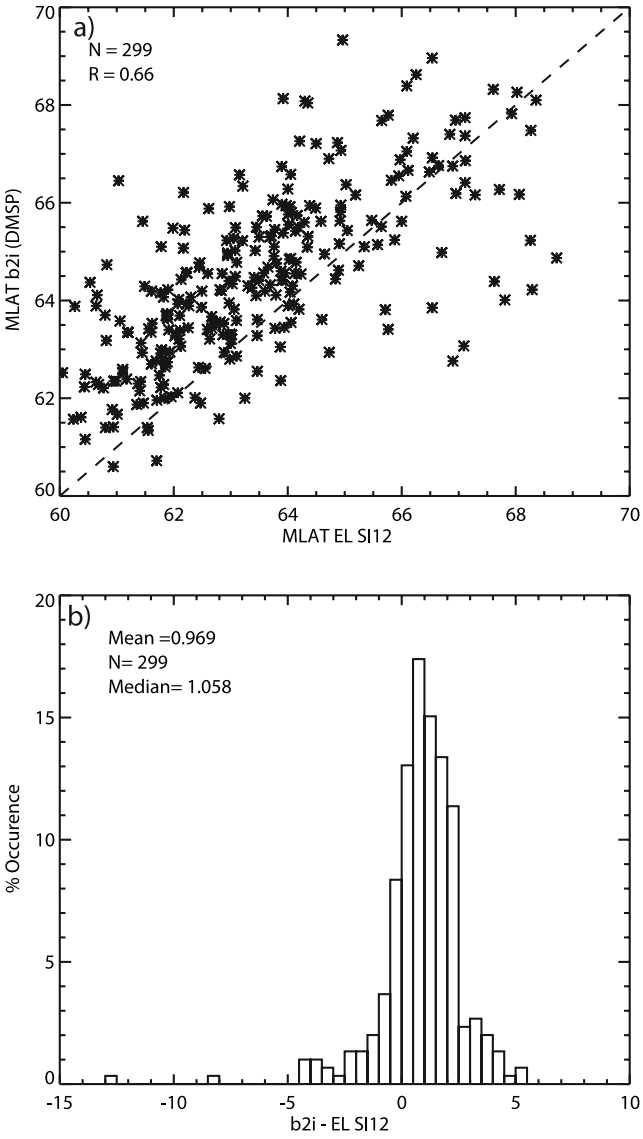

Figure 5. (a) Scatter plot of b2i obtained by DMSP and EL SI12. (b) Histogram of the difference between magnetic latitudes of b2i and EL.

sets of data are correlated and that the b2i position is an indicator of the magnetic field stretching reinforces the conclusion provided by GOES-8 data. The shift between EL and b2i was expected since b2i is defined as the region of maximum flux and EL is obtained with a shift of 1.4 σ equatorward of the maximum of the Gaussian curve. These two ways to determine the position of a proxy of IB are consistent with the shape of the profile observed by each satellite. The typical profile observed by the DMSP instrument is a gradual increase of the auroral intensity when the spacecraft moves equatorward, followed by a sudden drop off in the equatorial side of the emission region. Such a profile observed by SI12 is seen with more continuous variations, which allows the Gaussian fit approximation detailed above. The different profile shapes provided by these two instruments are hard to reconcile but could be

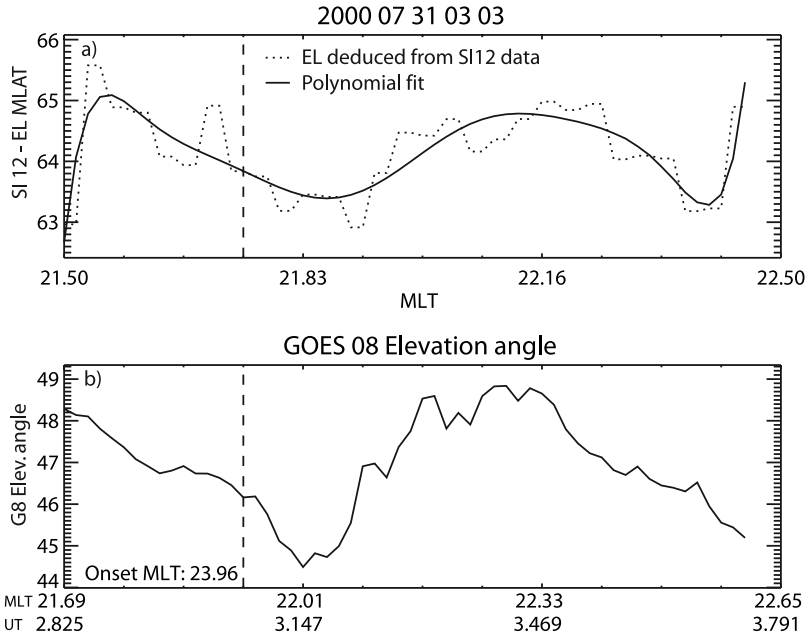

Figure 6. (a) The dotted line indicates the magnetic latitude of EL deduced from SI12 data at different times (and consequently, at different MLTs). The superposed solid line is a polynomial fit to the dotted line. The vertical dashed line indicates the time of onset. (b) Time evolution of the elevation angle deduced from GOES-8 measurements.

explained, at least partially, by the smoothing due to the point spread function of the SI12imager.

4. Application

[19] As an example of the possible application of this method, Figure 6 presents a comparison between results provided by the Donovan's algorithm applied to SI12 data and elevation angles deduced from GOES-8 measurements. Magnetic latitudes of EL are selected at the local time of the GOES-8 spacecraft. GOES-8 is located $\sim$2 MLT duskward of the onset position, which probably explains why the dipolarization occurs $\sim$5 minutes after onset. The trends presented by the two curves at Figure 6 are similar, even if high frequency details are not reproduced. We choose to represent the EL time evolution in Figure 6 with a polynomial fit, in order to reduce the impact of pointing uncertainties of the IMAGE spacecraft which affect the data set presented by the dashed curve in Figure 6a. The EL determination described above is now applied to the entire set of 259 substorm events. Figure 7 presents the time evolution of the EL position at different MLT's relative to onset (RMLT). The plots indicate the relative position of EL to a reference which is defined as the EL_Λ at the onset time and MLT. This reference is consequently defined separately for each individual event. These average results show that 60 minutes before onset, the EL curve between -3 and 3 RMLT is located at higher MLAT than the position where the onset will occur one hour later. The proton oval initiates an equatorward motion $\sim$30 minutes prior to the onset simultaneously in the 6 MLT regions around onset (between -3 and +3 RMLT – not shown). Before this equatorward motion starts, the IB was located almost symmetrically around the onset, with higher magnetic latitudes duskward and dawnward of the onset. Surprisingly, the slowest equatorward motion is observed at the onset local time. The equatorward motion speeds are $\sim$0.018 degree/min duskward of the onset position, $\sim$0.011 degree/min at onset MLT and $\sim$0.013 degree/min dawnward of the onset position. As a consequence of these different speeds at different RMLTs, the shape of the proton oval is not conserved during the event. The most equatorward magnetic latitude is reached during minutes following onset for the duskward region and during minutes preceding onset for the dawnward region. Following the equatorward motion, a poleward motion occurs and stops after $\sim$35 to 45 minutes after the onset.

[20] As easily seen in Figure 7, the evolution between 60 minutes before to 40 minutes after the onset changes from an almost symmetrical pattern of the EL location around the onset position (before onset) to an asymmetrical pattern with lower magnetic latitudes located duskward of the onset location. In spite of the weak intensity of variations in this statistical pattern, it is considered as a real effect since the large number of events used for this analysis. In order to evaluate if the asymmetry presented by Figure 7 has a counterpart in terms of magnetospheric stretching, Figure 8 presents the mean value of the elevation angles deduced from GOES-8 data. These data were recorded when GOES-8 was in the [-3, +3] RMLT region during each of selected events. During the period between 40 minutes to 20 minutes before the expansion phase onset, field line stretching plotted in Figure 8a presents a pattern almost symmetric with a stretching slightly more important (2 degrees) duskward of the onset. This can be considered as a level of reference. The dusk-dawn asymmetry is becoming more pronounced during the 15 minutes preceding the substorm onset (Figure 8a). After the onset (Figure 8b), the

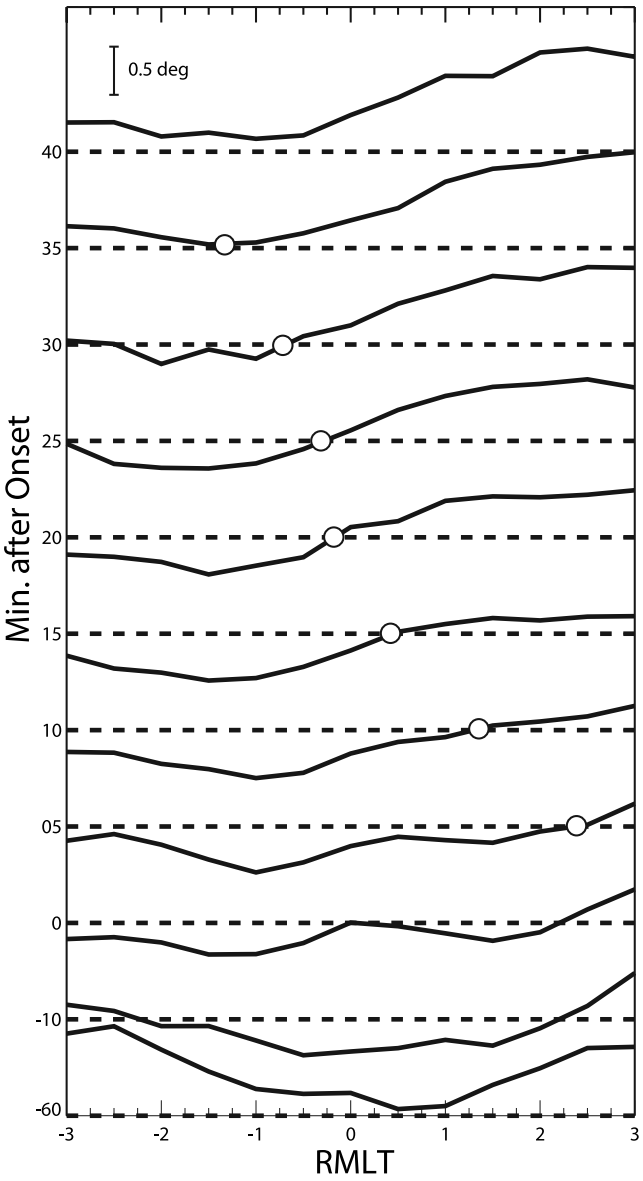

Figure 7. Superposed epoch analysis of the EL position for a set of 259 substorms. Each curve of this plot is the average of the 259 curves of the EL position relative to onset at different RMLT. Two curves are displayed for times before onset (60 and 10 minutes). After onset, one curve is displayed every 5 minutes. The scale of the variation's amplitudes is given in the top left of the panel. Negative values of RMLT are related to the onsets dusk side, positive values are related to the onsets dawn side.

largest stretching is located duskward of the onset position, which coincides with the most equatorward location of EL in Figure 7. A counterpart of the EL position observed in the dawn side of Figure 7 is visible in Figure 8, with a less stretched configuration in the [0, 3] RMLT sector. However, even if the trends are the same for these two variables, other mechanisms than pitch angle scattering due to field lines stretching may influence the EL position, especially during substorms [*Mende et al.*, 2002]. In spite of these different mechanisms which influence ionospheric proton precipitation (and thus the EL position) during active periods, it appears that, on a statistical basis, the position of EL is correlated with the magnetospheric topology.

[21] On a quantitative point of view, we can compare the amplitude displayed by Figure 7 and Figure 8 using the regression plotted on Figure 4. If we concentrate on the minutes just after onset, and compare the field line stretching 1 RMLT duskward the onset and 1 RMLT dawnward the onset, a difference of 5 degree is observed. Using the regression from Figure 4, a 5° difference at the GOES-8 position implies a 0.7° shift on the EL position. The actual variation given on Figure 7 is close to 0.4°. This difference suggests that the field line stretching is not the only factor influencing the EL position, but also that this linear model is not accurate enough. This question will be the cornerstone of our next study.

[22] These results are consistent with those presented by *Nagai* [1982], *Nagai* [1991] and *Trakhtengerts and Demekhov* [2005] and these studies provide an interesting context to the results presented here. *Nagai* [1991] observes an asymmetry in the dipolarization around midnight. The westward propagation of the current wedge described by *Nagai* [1982] may be compared to our results and associate the upward field aligned current region with the more important stretching and the more equatorward position of EL, and the less stretched magnetic field with the downward field aligned current region. In their discussion on the partial ring current during the main phase of magnetic storm, *Trakhtengerts and Demekhov* [2005] also noticed a strong azimutal asymmetry with ion fluxes peaked in the dusk MLT sector. The main cause of this asymmetry is the strengthening of the convection electric field which drives the bulk of ring current ions along open trajectories coming into the magnetosheath in the dusk sector. *Trakhtengerts and Demekhov* [2005] also indicate that plasma waves plays an important role in pitch angle scattering of ring current ions during substorm and consider the cyclotron instability of ring current ions as the main candidate to cause the pitch angle scattering and intense energetic ion precipitation in the dusk MLT region.

5. Conclusions

[23] In this study, we apply a Gaussian algorithm developed by *Donovan et al.* [2003] to data provided by the SI12 proton imager and determine the EL (equatorial limit) index. This algorithm was initially designed to use meridian scanning photometer data to identify the position of the optical b2i, which is considered as a good proxy of the isotropic boundary. To locate such a limit using only optical data implies that precipitated fluxes are mainly due to the magnetospheric configuration rather than processes acting along field lines between the source region and the ionosphere such as field aligned acceleration for example. This is likely during quiet activity periods but less obvious during active periods like substorm expansive phase. Consequently, the purpose is not to find a good proxy for IB but to investigate if the limit provided by the Donovan's algorithm applied on IMAGE/SI12 can be considered as a good tool to monitor magnetospheric stretching. By comparison with GOES-8 data, we find that the EL position is related to the stretching of the tail magnetic field. This

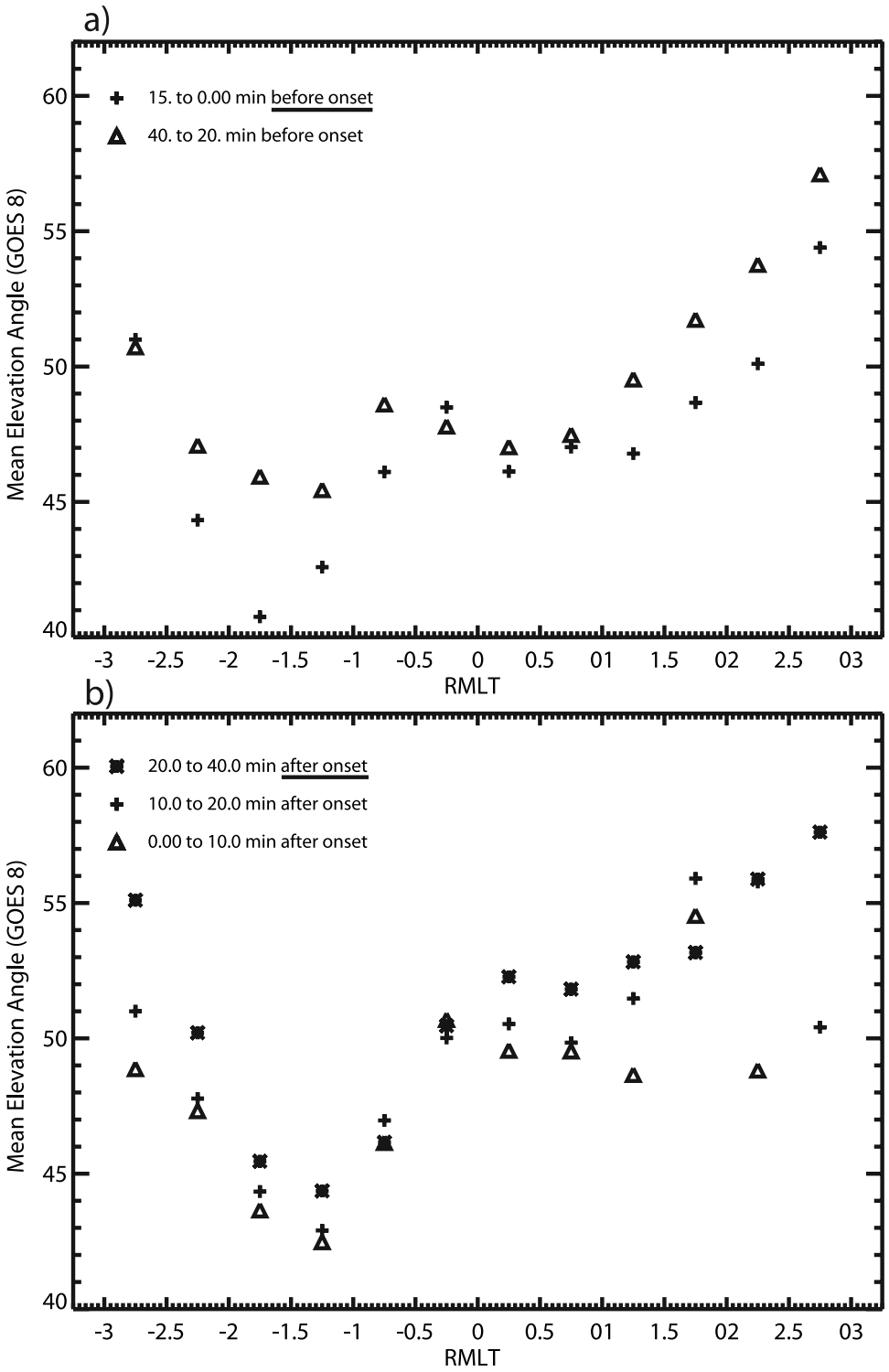

Figure 8. Statistical plot showing the RMLT (MLT relative to the onset position) dependence of the mean value of elevation angles deduced from GOES-8 during the growth phase (a) and the expansive phase (b) of 259 substorm events.

conclusion is reinforced by the similar shapes presented by the position of EL at different RMLT and different relative times from onset (Figure 7) and the mean value of elevation angles (Figure 8). EL positions are close to the b2i boundaries provided by DMSP instruments (Figure 5). The discrepancy is close to $\sim 1^\circ$ MLAT. Results presented in this paper indicates that:

[24] 1) In spite of various possible mechanisms acting between the tail and the ionosphere, the tail stretching has a strong enough relation with the proton auroral emission to

use these emissions as a stretching indicator, even during active periods such as substorm expansive phases.

[25] 2) Based on a large set of events, the magnetospheric configuration is more stretched duskward of the onset position during the expansive phase than dawnward. Based on the EL position – stretching relation displayed in Figure 3 and the time evolution shown at Figure 7, we suggest that the recovery of previously stretched configuration first occurs in the dawn sector and propagates to the dusk at a speed of $\sim$7 MLT/hour.

[26] **Acknowledgments.** M.M is supported by the AIF fellowship, J. C. G. and B. H. are supported by the Belgian National Fund for Scientific Research (FNRS). The IMAGE FUV investigation was supported by NASA through SWRI subcontract 83820 at the University of California, Berkeley, contract NAS5-96020. This work was funded by the PRODEX program of the European Space Agency (ESA) and the Fund for Collective and Fundamental Research (IISN grant 4.4508.06). We acknowledge data providers CDAWeb for the GOES data. The DMSP particle detectors were designed by Dave Hardy of AFRL, and data were obtained from JHU/ APL. We thank Dave Hardy, Fred Rich, and Patrick Newell for the use of the particle detectors.

[27] Wolfgang Baumjohann thanks Victor Sergeev and another reviewer for their assistance in evaluating this paper.

References

Blockx, C., J.-C. Gérard, M. Meurant, B. Hubert, and V. Coumans (2005), Far ultraviolet remote sensing of the isotropy boundary and magnetotail stretching, *J. Geophys. Res.*, *110*, A11215, doi:10.1029/2005JA011103.

Donovan, E. F., B. J. Jackel, I. Voronkov, T. Sotirelis, F. Creutzberg, and N. A. Nicholson (2003), Ground-based optical determination of the b2i boundary: A basis for an optical MT-index, *J. Geophys. Res.*, *108*(A3), 1115, doi:10.1029/2001JA009198.

Frey, H. U., S. B. Mende, V. Angelopoulos, and E. F. Donovan (2004), Substorm onset observations by IMAGE-FUV, *J. Geophys. Res.*, *109*, A10304, doi:10.1029/2004JA010607.

Gérard, J.-C., B. Hubert, A. Grard, M. Meurant, and S. B. Mende (2004), Solar wind control of auroral substorm onset locations observed with the IMAGE-FUV imagers, *J. Geophys. Res.*, *109*, A03208, doi:10.1029/2003JA010129.

Hubert, B., S. E. Milan, A. Grocott, S. W. H. Cowley, and J.-C. Gérard (2006), Dayside and nightside reconnection rates inferred from IMAGE-FUV and SuperDARN data, *J. Geophys. Res.*, *111*, A03217, doi:10.1029/2005JA011140.

Mende, S. B., et al. (2000), Far ultraviolet imaging from the IMAGE spacecraft. 1, System design, *Space Sci. Rev.*, *91*, 243.

Mende, S. B., H. U. Frey, T. J. Immel, D. G. Mitchell, C. son-Brandt, and J.-C Gérard (2002), Global comparison of magnetospheric ion fluxes and auroral precipitation during a substorm, *Geophys. Res. Lett.*, *29*(12), 1609, doi:10.1029/2001GL014143.

Mende, S. B., H. U. Frey, C. W. Carlson, J. McFadden, J.-C. Gérard, B. Hubert, S. A. Fuselier, G. R. Gladstone, and J. L. Burch (2002), IMAGE and FAST observations of substorm recovery phase aurora, *Geophys. Res. Lett.*, *29*(12), 1602, doi:10.1029/2001GL013027.

Nagai, T. (1982), Observed magnetic substorm signatures at synchronous altitude, *J. Geophys. Res*, *87*, 4405.

Nagai, T. (1987), Field-aligned currents associated with substorms in the vicinity of synchronous orbit, 2, Geos 2 and Geos 3 observations, *J. Geophys. Res.*, *92*, 2432.

Nagai, T. (1991), An empirical model of substorm related magnetic field variations at synchronous orbit, in Magnetospheric Substorms, *Geophys. Monogr. Ser.*, vol. 64, edited by J. R. Kan, T. A. Potemra, S. Kokubun, and T. Iijima, p. 91, AGU, Washington, D. C.

Newell, P. T., Y. I. Feldstein, Y. I. Galperin, and C. I. Meng (1996), Morphology of nightside precipitation, *J. Geophys. Res.*, *101*, 10,737.

Newell, P. T., V. A. Sergeev, G. R. Bikkuzina, and S. Wing (1998), Characterizing the state of the magnetosphere: Testing the ion precipitation maxima latitude (b2i) and the ion isotropy boundary, *J. Geophys. Res.*, *103*, 4739.

Sergeev, V. A., and B. B. Gvozdevsky (1995), MT-index—A possible new index to characterize the magnetic configuration of magnetotail, *Ann. Geophys.*, *13*, 1093.

Trakhtengerts, V. Y., and A. G. Demekhov (2005), Discussion paper: Partial ring current and polarization jet, *Geophys. Res. Lett.*, *5*, GI3007, doi:10.1029/2005GL000091.

Tsyganenko, N. A. (1989), A magnetospheric magnetic field model with a warped tail current sheet, *Planet. Space Sci.*, *37*, 5.

Tsyganenko, N. A. (1996), Effects of the solar wind conditions on the global magnetospheric configuration as deduced from data based field models, *Eur. Space Agency Spec. Publ., ESA*, *SP 389*, 181.

Tsyganenko, N. A. (2001), Empirical magnetic field models for the space weather program, in Space Weather, Geophys. Monogr. Ser., vol.125, edited by P. Song, H. Singer, and G. L. Siscoe, p. 273, AGU, Washington, D. C.

C. Blockx, V. Coumans, J.-C. Gérard, and B. Hubert, Laboratoire de physique atmosphérique et planétaire, Université de Liège, 17 Allée du 6 Août, 4000 Liège, Belgium.

M. Connors, Athabasca University, 11560 80 Avenue, Edmonton, T6G OR9, Canada.

E. F. Donovan, M. Meurant, and E. Spanswick, Institute for Space Research, University of Calgary, 2500 University Drive NW, Calgary, AB T2N 1N4, Canada. (matthieu@phys.ucalgary.ca)